LETTER

doi:10.1038/nature10732

Purkinje neuron synchrony elicits time-locked spiking in the cerebellar nuclei

Abigail L. Person[1]† & Indira M. Raman[1]

An unusual feature of the cerebellar cortex is that its output neurons, Purkinje cells, release GABA (γ-aminobutyric acid). Their high intrinsic firing rates[1] (50 Hz) and extensive convergence[2,3] predict that their target neurons in the cerebellar nuclei would be largely inhibited unless Purkinje cells pause their spiking, yet Purkinje and nuclear neuron firing rates do not always vary inversely[4]. One indication of how these synapses transmit information is that populations of Purkinje neurons synchronize their spikes during cerebellar behaviours[5–11]. If nuclear neurons respond to Purkinje synchrony, they may encode signals from subsets of inhibitory inputs[7,12–14]. Here we show in weanling and adult mice that nuclear neurons transmit the timing of synchronous Purkinje afferent spikes, owing to modest Purkinje-to-nuclear convergence ratios (~40:1), fast inhibitory postsynaptic current kinetics (τ_{decay} = 2.5 ms) and high intrinsic firing rates (~90 Hz). *In vitro*, dynamically clamped asynchronous inhibitory postsynaptic potentials mimicking Purkinje afferents suppress nuclear cell spiking, whereas synchronous inhibitory postsynaptic potentials entrain nuclear cell spiking. With partial synchrony, nuclear neurons time-lock their spikes to the synchronous subpopulation of inputs, even when only 2 out of 40 afferents synchronize. *In vivo*, nuclear neurons reliably phase-lock to regular trains of molecular layer stimulation. Thus, cerebellar nuclear neurons can preferentially relay the spike timing of synchronized Purkinje cells to downstream premotor areas.

During cerebellar behaviours, on-beam Purkinje cells fire synchronous simple spikes with millisecond-scale precision[5–8], and microbands of Purkinje cells fire synchronous complex spikes[9–11]. The extent to which cerebellar nuclear neurons respond to synchrony depends on the magnitude, convergence and kinetics of Purkinje inputs. We therefore measured these properties before assessing the consequence of Purkinje synchrony on nuclear firing *in vitro* and *in vivo*.

We first recorded IPSC amplitudes evoked in nuclear neurons by stimulating Purkinje axons in mouse cerebellar slices (Fig. 1a, b). Maximal stimulation evoked inhibitory postsynaptic currents (IPSCs) up to ~200 nS (mean ± s.e.m., 108.3 ± 13.0 nS; n = 17). Minimal stimulation evoked either failures or successes of 9.4 ± 1.0 nS (n = 30), the amplitudes of which resembled tetrodotoxin-sensitive spontaneous IPSCs[15], consistent with activation of a single fibre. The high unitary amplitude suggests that individual Purkinje-to-nuclear contacts are quite strong[16]. The maximal-to-minimal conductance ratio indicates that functional convergence in the slice is about 12, or maximally ~22. Because both slicing and incomplete recruitment of afferents probably limit maximal IPSC amplitudes, this estimate represents a lower bound on functional convergence in the intact cerebellar nuclei.

We obtained a second convergence estimate by considering structural constraints on innervation (see Supplementary Discussion for calculations). In mouse, the Purkinje-innervated surface of a large nuclear cell with four dendrites (3,130 μm^2) maximally accommodates 1,250 Purkinje boutons, each with a 2.5 μm^2 surface area; comparable numbers (600–1,200) are estimated for cat[17]. Multiple boutons must arise from a single Purkinje cell, however, because the quantal content of a unitary Purkinje IPSC[15,16] is 12–18. Given a boutonal release probability[18] of 0.5, each Purkinje cell must contribute ~24–36 boutons per target, predicting 34–52 Purkinje cells per nuclear cell.

A third convergence estimate was derived from the maximal $GABA_A$ receptor conductance per nuclear neuron[19], which yielded a mean convergence of ~20 (maximum, ~30) (Supplementary Discussion). The estimates from these three separate measures can be reconciled with classical histological measurements of 860 Purkinje cells per nuclear cell in the cat[3], by the observation that each Purkinje bouton has 9–10 synaptic densities[2,18]. Correcting for this factor reduces the predicted convergence to 86–96, on the order of magnitude of the present estimates. Thus, multiple approaches indicate a functional convergence in the intact cerebellum of tens of Purkinje neurons per nuclear neuron, probably 20–50 in the rodent.

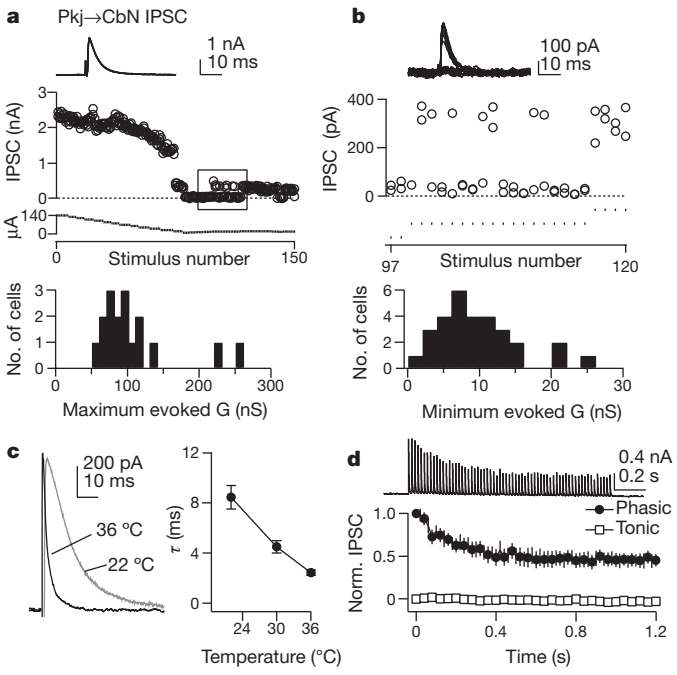

Figure 1 | Purkinje cell convergence and fast IPSCs in the cerebellar nuclei. **a**, IPSCs evoked by maximal stimulation. Holding potential, −57 mV (junction potential corrected). Top: five overlaid IPSCs. Middle: IPSC amplitudes as stimulus strength was reduced. Bottom: maximal conductances calculated from measured IPSC reversal potentials (n = 17, mean E_{Cl} = −75 mV). Bin width, 10 nS. CbN, cerebellar nuclei; Pkj, Purkinje. **b**, IPSCs evoked by minimal stimulation (range 16–20 μA). Top: 20 overlaid IPSCs. Middle: expansion of box in **a**. Events near the zero line fell within the noise. Bottom: minimal conductances (n = 30). Bin width, 2 nS. **c**, Left: scaled IPSCs in one cell at 22 °C and 36 °C. Right: temperature dependence of IPSC decay τ (n = 7). **d**, Top: 50-Hz train of IPSCs at 36 °C. Bottom: depression of phasic IPSCs and absence of tonic current during train. Data are mean ± s.e.m.

[1]Department of Neurobiology, Northwestern University, Evanston, Illinois 60208, USA. †Present address: Department of Physiology and Biophysics, University of Colorado School of Medicine, Aurora, Colorado 80045, USA.

Additional determinants of the efficacy of inhibition are the intrinsic firing rates and IPSC kinetics. In 17–26-day-old mice (P17–P26), nuclear neurons fired spontaneously at 91.5 ± 7.4 spikes s^{-1}, significantly faster than in P13 animals recorded under identical conditions[15] (22.0 ± 5.0 spikes s^{-1}; Supplementary Fig. 1), indicating a developmental increase in intrinsic firing rate. At near-physiological temperature (36 °C), the τ_{decay} of evoked IPSCs was 2.4 ± 0.2 ms (Fig. 1c), making corticonuclear IPSCs among the fastest known $GABA_A$-receptor-mediated currents[20]. This value is >5-fold briefer than the τ_{decay} of 13.6 ms of IPSCs at room temperature[21], which appears in previous corticonuclear models[12–14]. When unitary IPSCs were mimicked with dynamic clamp, the duration of inhibition of spontaneously firing nuclear cells varied directly with τ_{decay}[15,21,22], and the first post-inhibitory spike was well-timed relative to the stimulus[12,23] (Supplementary Fig. 2). Thus, brief IPSCs minimize inhibition.

When synchronous IPSCs were evoked at 50 Hz at 36 °C, peak IPSCs were depressed by 55% ($n = 6$), but the current decayed fully between stimuli (Fig. 1d), resulting in no accumulation of 'tonic' current[15]. Because tonic current is largely responsible for suppressing nuclear cell spiking, synchronous and asynchronous IPSCs may differentially modulate nuclear cell output. As a preliminary test of this idea, we delivered trains of dynamically clamped inhibitory postsynaptic potentials (dynIPSPs) from eight afferents, each with an amplitude of 10 nS and a rate of 50 Hz, which were either desynchronized (equivalent to one non-depressing input at 400 Hz) or synchronized (Fig. 2a). Not surprisingly, desynchronized dynIPSPs strongly inhibited spontaneous firing. In contrast, upon synchronization of dynIPSPs, nuclear neuron firing rates jumped instantaneously, but only when τ_{decay} was brief (Fig. 2b). Moreover, with physiological τ_{decay}, nuclear cell spiking entrained to the synchronous input, evident as a match between the instantaneous firing rate and the stimulus rate (Fig. 2a). Likewise, IPSPs evoked by Purkinje stimulation nearly perfectly entrained nuclear neuron spiking between 60 and 80 Hz (Fig. 2c, d); in contrast, desynchronized dynIPSPs suppressed firing at all stimulus rates (Fig. 2d). Thus, in the extreme case of low convergence, the output of nuclear neurons is determined by both the rate and synchrony of inhibition.

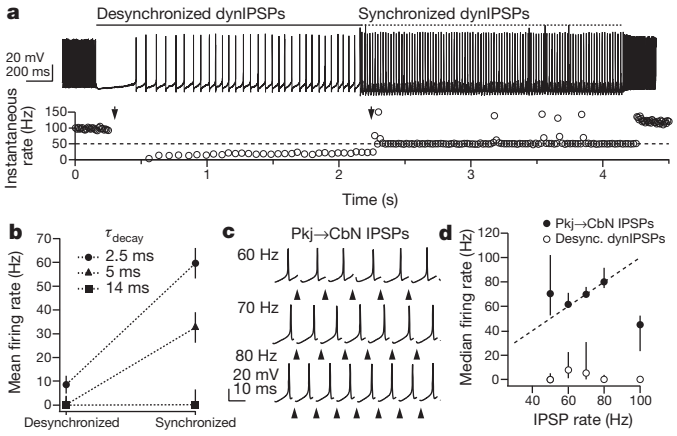

Figure 2 | Entrainment of nuclear neuron spiking to synchronous IPSPs. **a**, Top: response to desynchronized and synchronized dynIPSPs from 8 inputs at 50 Hz, τ_{decay} = 2.5 ms. Bottom: instantaneous firing rates of neuron in **a**, showing entrainment during synchrony. Arrows indicate onset of desynchronized (left) and synchronized (right) dynIPSPs. Tall spikes reflect overlapping dynIPSPs and spikes. **b**, Firing rates during desynchronized and synchronized 50-Hz trains with different dynIPSP kinetics (τ_{decay} = 2.5, 5, 14 ms, n = 25, 18, 10). **c**, Entrainment to corticonuclear IPSPs (36 °C) between 60 and 80 Hz. Arrowheads indicate stimulation times. **d**, Median firing rates (±1 quartile) in response to evoked IPSPs (closed symbols) and desynchronized dynIPSPs (open symbols). From 50–100 Hz, evoked, n = 8, 8, 8, 7, 3; simulated, n = 25, 10, 10, 9, 14. Dashed line indicates unity. Data are mean ± s.e.m., unless noted.

Synchronous Purkinje firing occurs *in vivo*[5–11], but the proportion of convergent Purkinje cells that synchronize is probably <100%. We therefore mimicked 40 Purkinje afferents with dynamic clamp, reflecting a realistic functional convergence, and tested whether synchronizing only a subpopulation of inputs can affect cerebellar nuclear output. To account for synaptic depression and mimic irregular spiking *in vivo*[23,24], each input was 5 nS, and inter-IPSP intervals were drawn from Gaussian distributions (coefficient of variation (CV) = 1), yielding a mean of 50 IPSPs s^{-1}. After 1 s of asynchronous inhibition, a fixed number of inputs (2–20, or 5–50%) was synchronized at 20–125 Hz, while the remaining inputs continued to provide asynchronous inhibition, each at 50 IPSPs s^{-1} (Fig. 3a, b). Asynchronous dynIPSPs greatly slowed nuclear cell firing. Firing rates, however, increased with fractional synchrony (Fig. 3a, c). The averaged voltage trajectories of synchronous dynIPSPs preceding and lacking a spike did not differ in the depth of hyperpolarization (Supplementary Fig. 3). Thus, the action potentials are not low-threshold spikes that follow unusually large inhibitory stimuli.

During trains of synchronous dynIPSPs, distinct temporal patterns of spiking emerged. For all frequencies tested, interspike interval distributions clustered at multiples of the interstimulus intervals of the synchronous dynIPSPs (Fig. 3d), reflecting phase locking of spikes to the regular stimulus train. The data were combined across stimulus

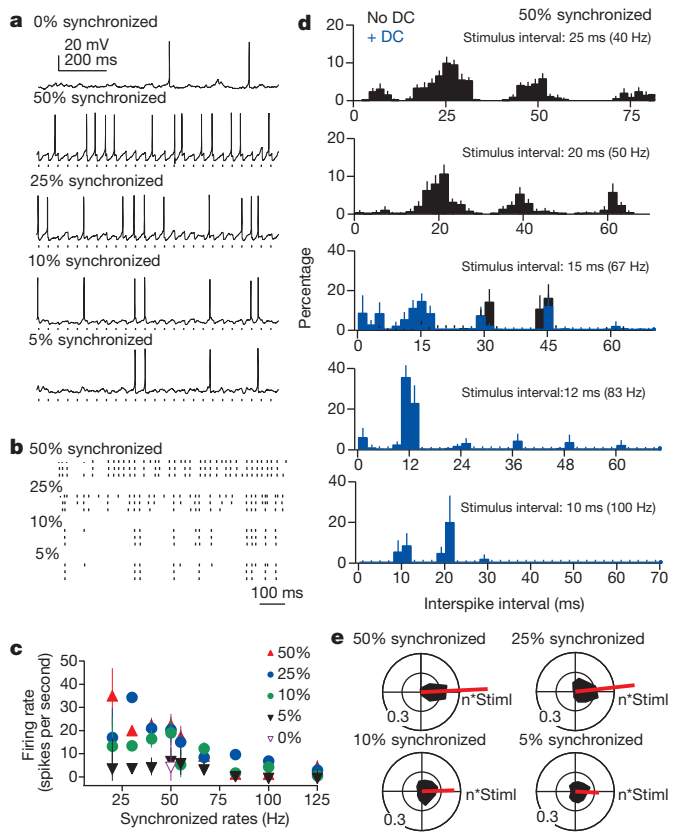

Figure 3 | The synchronous subpopulation of Purkinje inputs sets spike timing of nuclear neurons. **a**, Nuclear neuron responses to dynIPSPs from 40 asynchronous or partially synchronized inputs, as labelled. **b**, Spike rasters during dynIPSP trains with 50–5% synchrony. **c**, Firing rates during 20–125-Hz trains with 0–50% synchrony ('Synchronized rates'). **d**, Normalized interspike interval distributions during 50% synchrony, from 40 to 100 Hz. Abscissa tick marks indicate multiples of the interstimulus intervals. Bin width, 2 ms. Black, no current injection; blue, with 200 pA direct current (DC) applied to increase spike number during inhibition. **e**, Black: polar histograms of interspike intervals during 50–5% synchrony for 50, 55, 67, 83, 100 and 125 Hz input. Each cycle is one interstimulus interval (StimI). Red: net vectors of interspike interval histograms. (For 50%, 25%, 10%, 5% synchrony, n = 14, 9, 7, 7.) Data are mean ± s.e.m.

frequency by plotting interspike intervals as normalized polar histograms, with 0° representing multiples of the interstimulus interval (Fig. 3e). A net vector magnitude of 1 indicates perfect phase locking, and 0 indicates randomly occurring spikes. For all fractions of synchrony, the net vector was oriented close to 0° (2° ± 2°) with a non-zero magnitude (0.18, 0.25, 0.45 and 0.52 for 5%, 10%, 25% and 50% synchrony), illustrating the temporal restructuring of spike patterns according to stimulus interval.

To test whether conditions *in vivo* permit phase locking, we recorded single units from the cerebellar nuclei in anaesthetized adult mice (Fig. 4a). Purkinje spiking was partially synchronized by stimulating the molecular layer[23]. Indeed, for stimuli from 20–120 Hz, phase locking was robust in all neurons confirmed histologically to be within the nuclei (10 cells in 10 mice; Fig. 4a, b). No phase locking was apparent in two neurons located outside the nuclei. The net vector of the mean polar histogram combined across frequencies was oriented at −3° (Fig. 4c). Its magnitude (0.33) was between those for 10% and 25% synchrony *in vitro*, and was greater than that of baseline (0.09, $P < 0.05$, within-cell comparisons of vector magnitudes; direction 257°).

Stimulation modulated the mean firing rates of individual neurons ($P < 0.05$ versus baseline, within-cell comparisons). Like the results for different fractional synchrony *in vitro*, however, spike rates decreased in some cells ($n = 7$) and increased in others ($n = 3$; Supplementary Fig. 4), yielding no net change across cells ($P > 0.05$; Fig. 4d). Thus, the firing rate of nuclear cells, which is probably affected by both basal excitation and the fractional synchrony induced by the stimulus, does not obviously encode information about the rate of inhibitory inputs.

To evaluate whether stimulation directly excited nuclear neurons, we compared stimulus-to-spike latencies across conditions. *In vivo* latencies were 20.2 ± 2.2 ms, >5-fold greater than excitatory postsynaptic potential (EPSP)-to-spike latencies *in vitro* (3.5 ± 0.5, inhibition blocked), making direct excitation seem unlikely. Instead, *in vivo* latencies were closer to IPSP-to-spike latencies (11.9 ± 1.4 ms, excitation blocked) and synchronous dynIPSP-to-spike latencies with background inhibition (13.5 ± 0.6 ms; Fig. 4e), consistent with sequential parallel fibre and Purkinje cell activation[23]. Given the similarity of phase locking *in vivo* and *in vitro* with excitation blocked, these results suggest that the *in vivo* stimulation synchronizes Purkinje cell simple spikes, which in turn set the timing of nuclear cell spikes. The reliability of phase locking to regular trains of inhibitory stimuli *in vivo* further suggests that the spike patterns of a synchronized Purkinje subpopulation can be transmitted with fidelity by cerebellar nuclear neurons.

These experiments address the long-standing question in cerebellar physiology of how nuclear neurons encode signals from convergent, inhibitory Purkinje cells firing at high basal rates[1]. The intrinsic tendency of nuclear neurons to fire permits time-locked spiking during the transient reduction in inhibition after a few brief IPSCs overlap. Even synchrony of only two afferents (5%) can influence the timing of nuclear cell spiking. The results provide an alternative to the idea that nuclear cell firing requires pauses that permit low-threshold rebound spikes after prolonged Purkinje activity: not only would such a mechanism discard information present in graded Purkinje firing rates, but it would also introduce ~100-ms delays in cerebellar processing that are not evident[25].

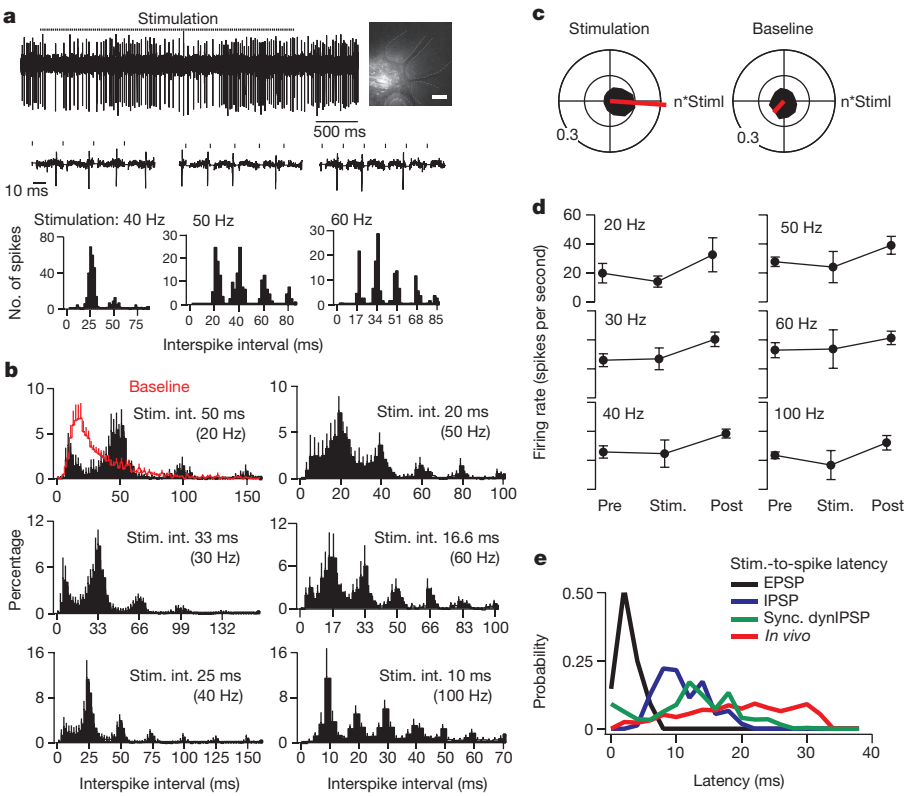

Figure 4 | Nuclear neurons phase-lock to molecular layer stimulation *in vivo*. **a**, Upper trace: response of a nuclear neuron to 40-Hz molecular layer stimulation (bar). Inset, recording site in the cerebellar nuclei recovered after focal Alexa 568 injection. Dashed lines demarcate cerebellar folia. Scale bar, 200 μm. Lower traces: expanded segments of spikes during 40-, 50- and 60-Hz stimulation (ticks), showing the long stimulus-to-spike latency. Stimulus artefacts are set to zero. Plots show interspike interval histograms for responses above. **b**, Mean normalized interspike interval distributions during molecular layer stimulation from 20 to 100 Hz for 4, 9, 9, 7, 5, and 7 cells respectively. Abscissa tick marks indicate multiples of the interstimulus interval. Red baseline histogram includes intervals before and after stimulation. Peaks at multiples of 8.3 ms were evident in 2 out of 2 cells stimulated at 120 Hz (not shown). Bin width, 2 ms. **c**, Black: polar histograms of interspike intervals during stimulation across rates (left) or during baseline periods. Red: net vectors of polar histograms. **d**, Mean firing rates before (Pre, 1 s), during (Stim., 3 s) and after (Post) stimulation. **e**, Stimulus-to-spike latencies for pharmacologically isolated EPSPs (black), IPSPs (blue) and dynIPSPs during partial synchrony (green) and *in vivo* (red). Data are mean ± s.e.m.

The extent to which time locking occurs during natural cerebellar processing will depend on the fractional synchrony of converging Purkinje cells, the precision of this synchrony, and the variance of ongoing excitation of nuclear neurons[13]. Supporting the idea that synchronized Purkinje neurons converge, simple spike synchrony is observed in neighbouring on-beam Purkinje cells[5,6], and closely spaced Purkinje cells probably converge on a common nuclear neuron[26]. Moreover, neighbouring Purkinje cells appear to be functionally related, as trans-synaptic tracing from muscles labels discrete strips of Purkinje cells[27].

A remaining question is how time-locked nuclear cell spikes are processed downstream. In the red nucleus, each interpositus axon makes parasagittally ramifying contacts[28], and about 50 interpositus neurons converge onto each target, producing EPSPs with little short-term plasticity[29]. Therefore, summation of EPSPs in the red nuclei may drive spiking that follows the firing pattern of the synchronized Purkinje subpopulation. More generally, time locking by cerebellar nuclear neurons may be a mechanism whereby the rate and timing of signals from varying groups of synchronized Purkinje cells are preferentially transmitted to premotor areas and other cerebellar targets.

METHODS SUMMARY

Procedures conformed to institutional guidelines for animal care and use.

***In vitro* electrophysiology.** Parasagittal cerebellar slices from both sexes of C57BL/6 13–29-day-old mice were cut[15] in artificial cerebrospinal fluid (ACSF; 35 °C). Recordings from large nuclear neurons were made[15] at 35–37 °C, unless noted, with a Multiclamp 700B amplifier and pClamp acquisition software. IPSCs were evoked in 6,7-dinitroquinoxaline-2,3-dione (DNQX; 5 μM), (*RS*)-3-(2-carboxypiperazin-4-yl)-propyl-1-phosphonic acid (CPP; 10 μM) and strychnine (2 μM) by 0.1-ms pulses delivered through a concentric bipolar electrode in the white matter surrounding the cerebellar nuclei. Evoked IPSCs were considered minimal when a fixed intensity stimulus elicited responses and failures with approximately equal likelihood, and maximal when increasing intensity produced no larger IPSCs. Dynamic clamp was implemented with an SM-2 (Cambridge Conductance) and a P25M real-time DSP board sampling between 10 and 25 kHz. Simulated IPSCs had a rise time and τ_{decay} of 0.1 and 2.5 ms, 0.5 and 5 ms, or 1 and 14 ms, and reversed at −75 mV. Desynchronized inputs had dynIPSP intervals distributed uniformly. Asynchronous dynIPSP intervals were drawn from a Gaussian distribution, created offline in IgorPro 5.05, with CV = 1. Forty independent trains were merged.

***In vivo* electrophysiology.** Adult C57BL/6 mice were anaesthetized with ketamine (80–100 mg kg^{-1}) and xylazine (5–10 mg kg^{-1}). A glass recording electrode containing 2 M NaCl was targeted to the cerebellar nuclei. A bipolar stimulating electrode (~300 μm between poles) was placed stereotaxically in the molecular layer, flanking the recording electrode. Three-second stimulus trains were delivered once every 15 s, repeated 4–20 times per frequency. Data were analysed in IgorPro.

Full Methods and any associated references are available in the online version of the paper at www.nature.com/nature.

Received 8 December 2010; accepted 23 November 2011.
Published online 25 December 2011.

1. Thach, W. T. Discharge of Purkinje and cerebellar nuclear neurons during rapidly alternating arm movements in the monkey. *J. Neurophysiol.* **31,** 785–797 (1968).
2. Chan-Palay, V. *Cerebellar Dentate Nucleus: Organization, Cytology, and Transmitters* (Springer, 1977).
3. Palkovits, M., Mezeky, E., Hamori, J. & Szentagothai, J. Quantitative histological analysis of the cerebellar nuclei in the cat. I. Numerical data on cells and on synapses. *Exp. Brain Res.* **28,** 189–209 (1977).
4. McDevitt, C. J., Ebner, T. J. & Bloedel, J. R. Relationships between simultaneously recorded Purkinje cells and nuclear neurons. *Brain Res.* **425,** 1–13 (1987).
5. Bell, C. C. & Grimm, R. J. Discharge properties of Purkinje cells recorded on single and double microelectrodes. *J. Neurophysiol.* **32,** 1044–1055 (1969).
6. Heck, D. H., Thach, W. T. & Keating, J. G. On-beam synchrony in the cerebellum as the mechanism for the timing and coordination of movement. *Proc. Natl Acad. Sci. USA* **104,** 7658–7663 (2007).
7. de Solages, C. *et al.* High-frequency organization and synchrony of activity in the Purkinje cell layer of the cerebellum. *Neuron* **58,** 775–788 (2008).
8. Wise, A. K., Cerminara, N. L., Marple-Horvat, D. E. & Apps, R. Mechanisms of synchronous activity in cerebellar Purkinje cells. *J. Physiol.* **588,** 2373–2390 (2010).
9. Welsh, J. P., Lang, E. J., Sugihara, I. & Llinas, R. Dynamic organization of motor control within the olivocerebellar system. *Nature* **374,** 453–457 (1995).
10. Ozden, I., Sullivan, M. R., Lee, H. M. & Wang, S. S. Reliable coding emerges from coactivation of climbing fibers in microbands of cerebellar Purkinje neurons. *J. Neurosci.* **29,** 10463–10473 (2009).
11. Schultz, S. R., Kitamura, K., Post-Uiterweer, A., Krupic, J. & Häusser, M. Spatial pattern coding of sensory information by climbing fiber-evoked calcium signals in networks of neighboring cerebellar Purkinje neurons. *J. Neurosci.* **29,** 8005–8015 (2009).
12. Gauck, V. & Jaeger, D. The control of rate and timing of spikes in the deep cerebellar nuclei by inhibition. *J. Neurosci.* **20,** 3006–3016 (2000).
13. Gauck, V. & Jaeger, D. The contribution of NMDA and AMPA conductances to the control of spiking in neurons of the deep cerebellar nuclei. *J. Neurosci.* **23,** 8109–8118 (2003).
14. Kistler, W. M. & De Zeeuw, C. I. Time windows and reverberating loops: a reverse-engineering approach to cerebellar function. *Cerebellum* **2,** 44–54 (2003).
15. Telgkamp, P. & Raman, I. M. Depression of inhibitory synaptic transmission between Purkinje cells and neurons of the cerebellar nuclei. *J. Neurosci.* **22,** 8447–8457 (2002).
16. Pedroarena, C. M. & Schwarz, C. Efficacy and short-term plasticity at GABAergic synapses between Purkinje and cerebellar nuclei neurons. *J. Neurophysiol.* **89,** 704–715 (2003).
17. Bengtsson, F., Ekerot, C.-F. & Jörntell, H. *In vivo* analysis of inhibitory synaptic inputs and rebounds in deep cerebellar nuclear neurons. *PLoS ONE* **6,** e18822 (2011).
18. Telgkamp, P., Padgett, D. E., Ledoux, V. A., Woolley, C. S. & Raman, I. M. Maintenance of high-frequency transmission at Purkinje to cerebellar nuclear synapses by spillover from boutons with multiple release sites. *Neuron* **41,** 113–126 (2004).
19. Pugh, J. R. & Raman, I. M. $GABA_A$ receptor kinetics in the cerebellar nuclei: evidence for detection of transmitter from distant release sites. *Biophys. J.* **88,** 1740–1754 (2005).
20. Bartos, M. *et al.* Fast synaptic inhibition promotes synchronized gamma oscillations in hippocampal interneuron networks. *Proc. Natl Acad. Sci. USA* **99,** 13222–13227 (2002).
21. Anchisi, D., Scelfo, B. & Tempia, F. Postsynaptic currents in deep cerebellar nuclei. *J. Neurophysiol.* **85,** 323–331 (2001).
22. Uusisaari, M. & Knopfel, T. GABAergic synaptic communication in the GABAergic and non-GABAergic cells in the deep cerebellar nuclei. *Neuroscience* **156,** 537–549 (2008).
23. Hoebeek, F. E., Witter, L., Ruigrok, T. J. & De Zeeuw, C. I. Differential olivo-cerebellar cortical control of rebound activity in the cerebellar nuclei. *Proc. Natl Acad. Sci. USA* **107,** 8410–8415 (2010).
24. Goossens, H. H. L. M. *et al.* Simple spike and complex spike activity of floccular Purkinje cells during the optokinetic reflex in mice lacking cerebellar long-term depression. *Eur. J. Neurosci.* **19,** 687–697 (2004).
25. Mauk, M. D. & Buonomano, D. V. The neural basis of temporal processing. *Annu. Rev. Neurosci.* **27,** 307–340 (2004).
26. Sugihara, I. *et al.* Projection of reconstructed single Purkinje cell axons in relation to the cortical and nuclear aldolase C compartments of the rat cerebellum. *J. Comp. Neurol.* **512,** 282–304 (2009).
27. Ruigrok, T. J. H., Pijpers, A., Goedknegt-Sabel, E. & Coulon, P. Multiple cerebellar zones are involved in the control of individual muscles: a retrograde transneuronal tracing study with rabies virus in the rat. *Eur. J. Neurosci.* **28,** 181–200 (2008).
28. Shinoda, Y., Futami, T., Mitoma, H. & Yokota, J. Morphology of single neurons in the cerebello-rubrospinal system. *Behav. Brain Res.* **28,** 59–64 (1988).
29. Toyama, K., Tsukahara, N., Kosaka, K. & Matsunami, K. Synaptic excitation of red nucleus neurones by fibres from interpositus nucleus. *Exp. Brain Res.* **11,** 187–198 (1970).

Supplementary Information is linked to the online version of the paper at www.nature.com/nature.

Acknowledgements We are grateful to J. R. Pugh for new analysis of data from ref. 19 on whole-cell GABA conductances. We thank D. Ferster, D. McLean and C. Woolley for comments on the manuscript. This work was supported by NIH grants R01-NS39395 (I.M.R.) and F32-NS067831 (A.L.P.).

Author Contributions A.L.P. performed all experiments and analyses. A.L.P. and I.M.R. designed and interpreted experiments and wrote the manuscript.

Author Information Reprints and permissions information is available at www.nature.com/reprints. The authors declare no competing financial interests. Readers are welcome to comment on the online version of this article at www.nature.com/nature. Correspondence and requests for materials should be addressed to I.M.R. (i-raman@northwestern.edu) or A.L.P. (a-person@northwestern.edu).

METHODS

Tissue preparation. Parasagittal slices of the cerebellar nuclei were prepared as in ref. 15 in accordance with institutional guidelines for animal care and use. P13–P29 mice were deeply anaesthetized with isofluorane and transcardially perfused with warm (35 °C) ACSF containing (in mM): 123 NaCl, 3.5 KCl, 26 $NaHCO_3$, 1.25 NaH_2PO_4, 1.5 $CaCl_2$, 1 $MgCl_2$, 10 glucose and equilibrated with 95/5% O_2/CO_2. Mice were then rapidly decapitated and the brains removed into ACSF (35 °C). Slices (300 μm thick) were cut on a Vibratome (Leica VT 100S) and incubated in warmed (35 °C), oxygenated ACSF for at least 1 h before recording.

Electrophysiological recording. Cerebellar slices were transferred to a recording chamber perfused continuously with warmed (35–37 °C, unless noted), oxygenated ACSF at a flow rate of 2–4 ml min^{-1}. Slices were visualized with infrared differential interference contrast microscopy and recordings were made from large neurons (soma diameters >15 μm). Neurons all had fast decay constants (~2.5 ms at 36°C) resembling the <5 ms τ_{decay} of glutamic acid decarboxylase (GAD)-negative large neurons at 34 °C rather than the ~10 ms τ_{decay} of GAD-positive neurons[22]. They are therefore likely to be excitatory projection neurons. Data were filtered at 6 kHz and sampled at 10–25 kHz.

Voltage- and current-clamp recordings were made with a Multiclamp 700B amplifier (Molecular Devices) and pClamp 10.0 data acquisition software (Molecular Devices). Borosilicate patch pipettes were pulled to tip resistances of 2–4 MΩ and filled with an internal solution containing (mM): 130 K-gluconate, 2 Na-gluconate, 6 NaCl, 10 HEPES, 2 $MgCl_2$, 0.1 or 1 EGTA, 14 Tris-creatine phosphate, 4 MgATP, 0.3 Tris-GTP and 10 sucrose. For experiments isolating $GABA_A$-receptor-mediated currents, DNQX (5 μM), CPP (10 μM) and strychnine (2 μM) were included in the bath solution and currents were evoked by stimulating the white matter surrounding the cerebellar nuclei with 0.1-ms current pulses (Isoflex Stimulus Isolation Unit; AMPI) delivered through a concentric bipolar electrode (FHC). Evoked IPSCs were considered minimal when a fixed amplitude stimulus strength elicited IPSCs or failures with approximately equal likelihood, indicating that stimulation was at threshold for a single input.

Dynamic clamp was implemented with a SM-2 system (Cambridge Conductance) with a P25M real-time DSP board (Innovative Integration) sampling between 10 and 25 kHz. Unitary conductances were set at either 10 or 5 nS and three kinetic profiles were used: 0.1-ms rise time and a single exponential τ_{decay} of 2.5 ms; 0.5-ms rise time and τ_{decay} of 5 ms (ref. 15); and 1-ms rise time and τ_{decay} 14 ms (ref. 21), with a reversal potential of −75 mV, accounting for a 7-mV measured liquid junction potential. In experiments manipulating synchrony between 0% and 100%, eight 10-nS convergent units were simulated. Desynchronized inputs were designed to distribute IPSP times uniformly during the inter-stimulus-interval, such that each 'unit' was activated at a given rate but offset in time by (inter-stimulus-interval/8) milliseconds. Gaussian trains were created offline in IgorPro 5.05 (Wavemetrics). Spike times were drawn from a Gaussian distribution with a CV of 1. Forty independent trains were merged to represent a population of corticonuclear IPSP arrival times and applied to trigger inhibitory conductances.

***In vivo* electrophysiology.** Adult C57BL/6 mice were anaesthetized with a cocktail of 80–100 mg kg^{-1} ketamine and 5–10 mg kg^{-1} xylazine intraperitoneally. A small craniotomy above the cerebellum was made with a dental drill. A glass recording electrode containing 2 M NaCl with 1% Alexa 568 10K dextran amine was targeted to the cerebellar nuclei (in mm: 2.6–3.0 posterior to Lambda, 1.0–1.3 lateral, 2.2–3.1 depth). A bipolar stimulating electrode (~300 μm between poles) was placed stereotaxically in the cerebellar molecular layer, aligned approximately in the coronal plane (on-beam), flanking the recording electrode. Stimulus trains were 3 s, delivered once every 15 s, had pulse durations of 0.1 ms and amplitudes of 40 ($n = 1$), 200 ($n = 6$) or 360 μA ($n = 5$), after other studies that used 100–200 μA (ref. 23). A stimulus of 360 μA is expected to stimulate a sphere with <0.5 mm radius[30]. Each stimulus rate was delivered between 4 and 20 times to each unit. After each recording, dye was pressure injected to mark the recording site. Only one cell was recorded from each mouse. Mice were transcardially perfused with physiological saline, brains were collected and fixed in 4% paraformaldehyde. Brains were cryoprotected in 30% sucrose, sectioned to 40 μm on a freezing microtome, and visualized on a Leica laser scanning confocal microscope.

Data analysis. Data were analysed offline in IgorPro 5.05 (Wavemetrics). Statistical analysis was done with paired or unpaired two-tailed *t*-tests as noted in the text, with significance taken as $P < 0.05$. Polar plots were constructed by binning interspike intervals with bin size = stimulus interval/12 for each stimulus frequency in each cell and averaging first across cells and then across frequencies. On each polar plot, one cycle is one interstimulus interval, such that a bar at 0° indicates spikes occurring at multiples of the interspike interval. Net vector magnitudes and directions were computed by summing the x and y values associated with the angle and radius values of the 12 vectors (histogram bars) that compose the mean polar plot. The null polar plot for the *in vivo* data was constructed from the interspike intervals of spikes occurring during non-stimulated periods, plotted with the same time bases as the stimulated interspike intervals. For statistical comparison of stimulated and null interspike intervals *in vivo*, vector magnitudes were calculated for data binned at 0.1 ms.

30. Tehovnik, E. J., Tolias, A. S., Sultan, F., Slocum, W. M. & Logothetis, N. K. Direct and indirect activation of cortical neurons by electrical microstimulation. *J. Neurophysiol.* **96,** 512–521 (2006).